



## Density-Functional Theory and Experimental Evaluation of Inhibition Mechanism of Novel Imidazo[4,5-b]pyridine Derivatives

K. Bouayad<sup>1,2</sup>, Y. Kandri Rodi<sup>1</sup>, H. Elmsellem<sup>3\*</sup>, I. Abdel-Rahman<sup>4</sup>,  
E.H. El Ghadraoui<sup>2</sup>, S. Chakroune<sup>1</sup>, E. M. Essassi<sup>5</sup>

<sup>1</sup>Laboratory of Applied Organic Chemistry Sidi Mohamed Ben Abdellah University, Faculty of Sciences and Technology of Fez, Morocco.

<sup>2</sup>Laboratoire de Chimie de la matière condensée, Faculté des Sciences et Techniques Université Sidi Mohamed Ben Abdallah, Fès Morocco

<sup>3</sup>Laboratoire de chimie analytique appliquée, matériaux et environnement (LC2AME), Faculté des Sciences, B.P. 717, 60000 Oujda, Morocco.

<sup>4</sup>Department of Chemistry, College of Sciences, University of Sharjah, PO Box: 27272, UAE.

<sup>5</sup>Laboratoire de Chimie Organique Hétérocyclique, URAC, Université Mohamed V, Faculté des Sciences, Avenue Ibn-Batouta, Rabat, Morocco.

Received 22 Jun 2016,  
Revised 21 Oct 2016,  
Accepted 25 Oct 2016

### Keywords

- ✓ Imidazo[4,5-b]pyridine,
- ✓ Corrosion,
- ✓ HCl,
- ✓ inhibition,
- ✓ DFT,

[h.elmsellem@gmail.com](mailto:h.elmsellem@gmail.com) ;  
Phone: +212600254809;

### Abstract

The corrosion inhibition properties of two imidazo[4,5-b]pyridine derivatives namely, 1-allyl-6-bromo-2-methyl-1H-imidazo[4,5-b]pyridine (**KA-2**) and 6-bromo-2-methyl-1-(prop-2-ynyl)-1H-imidazo[4,5-b]pyridine (**KA-3**) for mild steel in 1.0 M HCl at 308 K were studied using density functional theory, weight loss measurements and electrochemical techniques. The obtained experimental results showed that the imidazo[4,5-b]pyridine derivatives are excellent inhibitors and their adsorption on the metal surface was found to follow the Langmuir adsorption model. Electrochemical findings revealed that the imidazo[4,5-b]pyridine derivatives act as a cathodic-type inhibitor. These inhibitors increase the polarization resistance and simultaneously decrease the double layer capacitance, which confirm their high ability to protect the metal against dissolution. The mechanism of inhibition of the studied imidazo[4,5-b]pyridine derivatives was discussed in the light of the DFT simulations studies. The theoretical results agree well with the experimental ones.

## 1. Introduction

Mild steel is the most common type among steels due to its exceptional mechanical properties and reduced price [1]. It has low carbon content (up to 0.3%) and it is used where large amounts of steel are necessary, and has found applications in many oil and gas industries for casing the down hole and in transmission pipelines [2]. The mild steel is very reactive as it reverts back to iron oxide when water, oxygen and ions are present [3]. Thus they are more vulnerable to corrosion which leads to great waste of natural resources and even causes potential risks. Further continual usage of hydrochloric and sulphuric acids for various industrial processes such as iron pickling, descaling practice in boilers, acidification of oil well in petroleum explorations etc., [2, 4].

The interfacial behavior of organic compounds can be modeled by modifying substituent and functional groups. Molecules that are otherwise only physically attached to the metal surface can be changed into chemically adsorbed entities. This is of particular significance in the field of corrosion inhibitors.

The correlation between the inhibitor efficiency and the molecular structure of organic compounds has been extensively investigated [5-8].

Availability of non-bonded (lone pair) and  $\pi$ -electrons in inhibitor molecules facilitates electron transfer from the inhibitor to the metal. A coordinate covalent bond involving transfer of electrons from inhibitor to the metal surface may be formed [9]. The strength of the chemisorption bond depends upon the electron density on the donor atom of the functional group and also upon the polarizability of the group.

Corrosion inhibitors are chemical compounds which when added in small concentrations to the environment minimize or prevent corrosion [10]. The use of environmental friendly inhibitors has become the need of an

hour. These inhibitors mainly inhibit corrosion by adsorption mechanism. In this case, the extent of inhibitor adsorption varies considerably with the presence of some physicochemical properties in the inhibitor, like the nature of functional groups, steric factors, the electronic distribution, planar structure, the presence of donor heteroatoms, such as N, O and S as well as the presence of unsaturated carbon bonds and aromatic rings [11, 12].

In view of the dominant role of environmental considerations, the main efforts of this current research is to choose corrosion inhibitors that contain more heteroatoms and/or long carbon chain systems with aromatic rings in their structure that are highly efficient even at very low concentrations [13, 14].

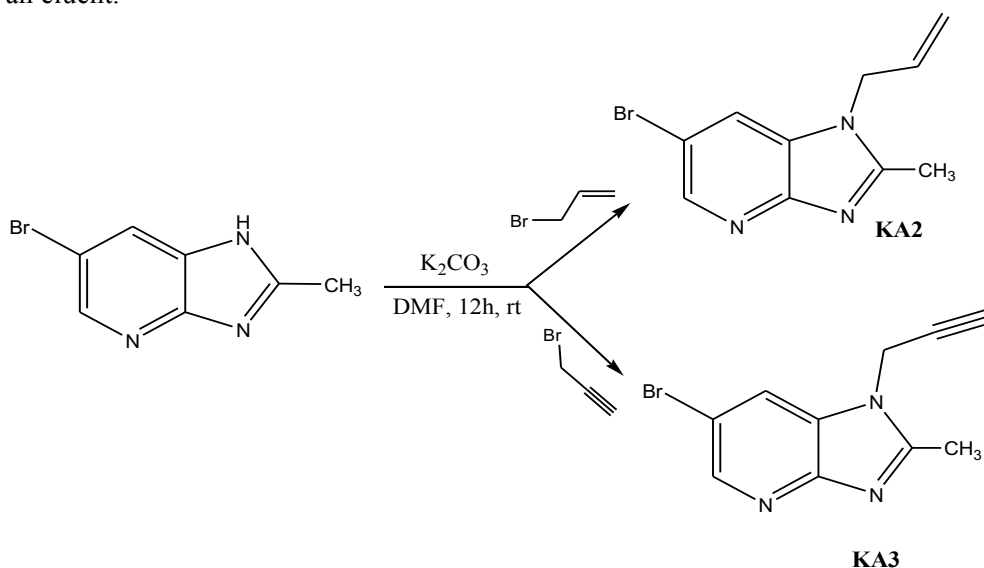
This study aims to continue the previous investigation of imidazo[4,5-b]pyridine derivatives as possible corrosion inhibitors [15] for mild steel in 1.0 M HCl solutions. Measurements were conducted using several corrosion monitoring techniques, such as weight loss, potentiodynamic polarization, and electrochemical impedance spectroscopy (EIS). In addition to that, this paper elucidates the adsorption behavior of some imidazo[4,5-b]pyridine derivatives on the mild steel surface using DFT simulations.

## 2. Material and Methods

The imidazo[4,5-b]pyridine unit is an important heterocyclic nucleus found in a large number of molecules in medicinal chemistry. Heterocycles derived from such compounds possess useful medicinal properties. Owing to their importance, strategies have been developed for their synthesis. Additionally, imidazo[4,5-b]pyridine derivatives have shown corrosion inhibition properties [16,17]. Hence, the synthesis of imidazo[4,5-b]pyridine derivatives represents nowadays an important topic in organic synthesis.

### 2.1. Inhibitors synthesis

A mass of 0.5 g (2.35 mmol) of 6-bromo-2-methyl-1H-imidazo[4,5-b]pyridine was dissolved in DMF (20 ml) in an Erlenmeyer flask. Potassium carbonate, 0.42 g (3.06 mmol), tetra-n-butyl ammonium bromide 0.04 g (0.1 mmol) and an alkylated agent, allyl bromide (KA2) or 3-bromo-1-propyne (KA3) (2.82 mmol) were added to the previous flask, as shown in Scheme 1. The reaction mixture was stirred for 12 hours at room temperature. The reaction mixture was filtered by suction filtration. The solvent was removed under reduced pressure. The residue was chromatographed on a column of silica gel using ethyl acetate-hexane with a composition of (1:2) by volume as an eluent.



**Scheme 1:** Synthesis of imidazo[4,5-b]pyridine derivatives (KA2 and KA3)

### 2.2. Materials

Mild steel specimens with composition (wt %) Fe 99.30%, C 0.076%, Si 0.026%, Mn 0.192%, P 0.012%, Cr 0.050%, Ni 0.050%, Al 0.023%, and Cu 0.135%, were polished with 600-1200 grade SiC Emery papers, washed with double distilled water, degreased with acetone in ultrasonic bath and finally allowed to dry in hot air. The gravimetric experiments were performed on mild steel specimens having dimension of  $1.5 \times 0.2 \times 1.5 \text{ cm}^3$ , whereas mild steel specimens with an expose area of  $1 \text{ cm}^2$  were used as working electrode for all electrochemical measurements. All the gravimetric and electrochemical experiments were performed in 1.0 M HCl solutions that prepared from the AR-grade HCl reagent (35%, Merck) and double distilled water.

### 2.3. Gravimetric measurements

The gravimetric experiments were performed as described previously [18]. All experiments were triply performed and the mean values were reported. The corrosion rate  $C_R$  ( $\text{mg cm}^{-2} \text{h}^{-1}$ ) was calculated using the following relation:

$$C_R = \frac{W}{At} \quad (1)$$

Where  $W$  is the average weight loss of three parallel mild steel strips,  $A$  is the exposed area of mild strip and  $t$  is the immersion time (6 hours). From the corrosion rate ( $C_R$ ), the inhibition efficiency ( $\eta$  %) and the surface coverage ( $\theta$ ) values were calculated using the following relationship:

$$\eta\% = \frac{C_R - C_{R(i)}}{C_R} \times 100 \quad (2)$$

$C_R$  and  $C_{R(i)}$  are the corrosion rate values in the absence and presence of the studied inhibitors, respectively.

#### 2.4. Electrochemical measurements

The electrochemical study was carried out using a potentiostat PGZ100 piloted by Voltmaster soft-ware. This potentiostat is connected to a cell with three electrode thermostats with double wall. A saturated calomel electrode (SCE) and platinum electrode were used as reference and auxiliary electrodes, respectively. Anodic and cathodic potentiodynamic polarization curves were plotted at a polarization scan rate of 0.5mV/s. Before all experiments, the potential was stabilized at free potential during 30 min. The polarisation curves are obtained from  $-800$  mV to  $-200$  mV at 308 K. The solution test is there after de-aerated by bubbling nitrogen. The electrochemical impedance spectroscopy (EIS) measurements are carried out with the electrochemical system, which included a digital potentiostat model Voltalab PGZ100 computer at  $E_{\text{corr}}$  after immersion in solution without bubbling. After the determination of steady-state current at a corrosion potential, sine wave voltage (10 mV) peak to peak, at frequencies between 100 kHz and 10 mHz are superimposed on the rest potential. Computer programs automatically controlled the measurements performed at rest potentials after 0.5 hour of exposure at 308 K. The impedance diagrams are given in the Nyquist representation. All experiments were repeated three times to ensure the reproducibility of the results.

### 3. Results and discussion

#### 3.1 Chemical methods

##### 3.1.1 Weight loss measurements

Fig. 2 shows the variation of the corrosion rate (in  $\text{mg cm}^{-2} \text{h}^{-1}$ ) of a mild steel electrode in 1.0 M HCl solutions without and with various concentrations of the KA2 and KA3 inhibitors at 308 K. The weight loss per unit time per unit area ( $\text{mg cm}^{-2} \text{h}^{-1}$ ), represents the corrosion rate of mild steel at the specified conditions. The rate of corrosion of the mild steel electrode decreases with increasing the inhibitor concentration, as indicated in Table 1. This behavior is also clearly seen in Fig. 2. This trend may result from the fact that both the adsorption and the surface coverage ( $\theta$ ) increase with the increase in the concentration of both inhibitors (KA2 and KA3).

From Table 1, the corrosion rate decreases with the addition of the inhibitor and in turn the inhibition efficiency ( $E_w\%$ ) increases to attain a maximum value of 87% and 90% at a concentration of  $10^{-3}$  M of KA2 and KA3 inhibitor, respectively. So it is obviously noticed that KA3 is a better corrosion inhibitor compared to KA2.

##### 3.1.2 Adsorption considerations

Adsorption considerations play an important role in explaining the relationship between the mild steel and the inhibitor. Adsorption characteristics are best explained using the surface coverage ( $\theta$ ) data. Once the fraction of surface covered has been obtained as a function of the concentration at constant temperature, adsorption isotherm could be estimated at equilibrium conditions [19]. Langmuir isotherm assumes presence of equivalent adsorption sites and that particle binding take place independently irrespective of nearby of adsorption sites being occupied or not [20]. Perfect linear plots were obtained (Fig. 3) on plotting  $C/\theta$  versus  $C$ , proposing that both of the studied inhibitors obey Langmuir isotherm:

$$\frac{C_{(\text{inh})}}{\theta} = \frac{1}{K_{(\text{ads})}} + C_{(\text{inh})} \quad (3)$$

Where C is the concentration of inhibitor (M), K is the adsorption–desorption equilibrium constant and  $\theta$  is the surface coverage, which is given by:

$$\theta = \% \eta / 100 \quad (4)$$

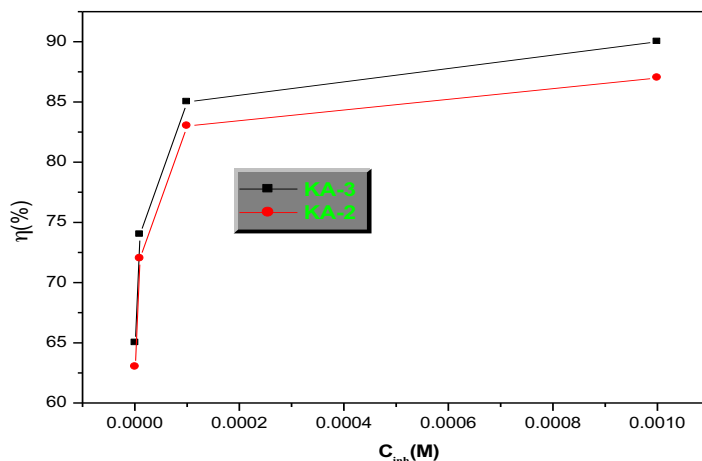


**Figure 2:** variation of the inhibition efficiency of mild steel corrosion in 1.0 M HCl solution in the absence and presence of various concentrations of KA2 and KA3 at 308 K.

**Table1:** The corrosion rate and the inhibition efficiency values in the absence and presence of KA2 and KA3 in 1.0 M HCl

Inhibitor Concentration	C (mol/l)	$C_R$ ( $\text{mg.cm}^{-2}\text{h}^{-1}$ )	$\eta$ (%)	$\theta$
1.0 M HCl	--	0.820	--	--
KA-2	$10^{-6}$	0.302	63	0.63
	$10^{-5}$	0.231	72	0.72
	$10^{-4}$	0.139	83	0.83
	$10^{-3}$	0.104	87	0.87
KA-3	$10^{-6}$	0.292	65	0.65
	$10^{-5}$	0.213	74	0.74
	$10^{-4}$	0.125	85	0.85
	$10^{-3}$	0.083	90	0.90

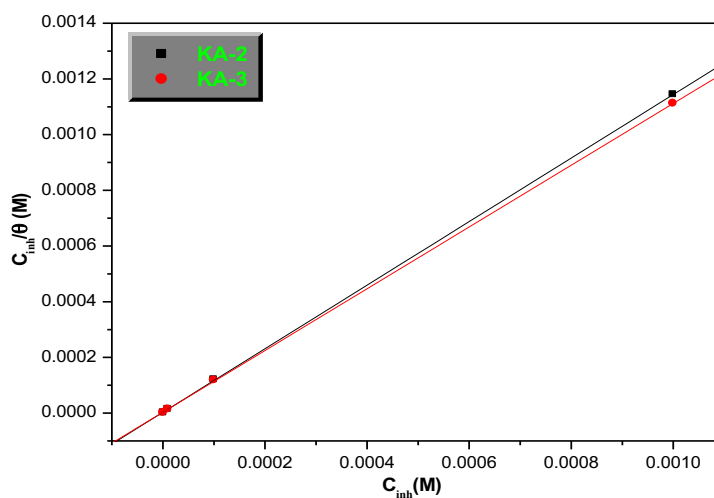


**Figure 3:** Langmuir adsorption isotherm model for mild steel in 1.0 M HCl solutions containing various concentrations of KA2 and KA3 inhibitors at 308 K.

The correlation coefficient ( $R^2$ ) values (from plot) being close to unity point toward (Table 2) the interaction between the adsorbed species on the metal surface and adsorbed organic molecules on the anodic and cathodic sites of the metal. Therefore, the adsorption of KA2 and KA3 molecules on the mild steel surface takes place via subsequent replacement of the adsorbed water molecules on the mild steel surface with KA2 and KA3 molecules in the solution as given below [21].



where  $n$  is total number of water molecules replaced by one molecule of KA2 or KA3 from the mild steel surface, commonly known as size ratio. It gives fundamental information about the interaction between the mild steel surface and the studied inhibitors KA2 and KA3.

The relationship between the adsorption constant and the change in the standard free energy of adsorption ( $\Delta G_{\text{ads}}$ ) was represented by the following equation [22]:

$$K_{\text{ads}} = \frac{1}{55.5} \exp\left(\frac{-\Delta G_{\text{ads}}^{\circ}}{RT}\right) \quad (5)$$

where  $R$  is the gas constant,  $T$  is the absolute temperature and 55.5 represent the concentration of water in acid solution ( $\text{mol}/\text{dm}^3$ ). The values of the change in the standard free energy of adsorption ( $\Delta G_{\text{ads}}$ ) at optimum concentration ( $10^{-3}$  M) of KA2 and KA3 inhibitors are given in Table 2.

**Table 2:** Parameters of the straight lines plot of  $C/\theta$  versus  $C$  in 1.0 M HCl solutions at 308 K.

$Y = A + B * X$	Correlation Coefficient ( $R^2$ )	Slope	$K$ ( $\text{M}^{-1}$ )	$\Delta G_{\text{ads}}^{\circ}$ ( $\text{KJ}.\text{mol}^{-1}$ )
KA2	0.99999	1.1412	3.46E+05	-42.93
KA3	0.99999	1.1088	3.20E+05	-42.73

From table.2, it is obvious that the values of  $\Delta G_{\text{ads}}^{\circ}$  are negative in the presence of the inhibitors (KA2 and KA3) which means that the adsorption of these inhibitors on the mild steel surface is a spontaneous process and they form a strong film on the mild steel surface [23]. Moreover, literature studied reveals that if the value of  $\Delta G_{\text{ads}}$ , is equal to -20 kJ/mol or less in negative value, this means that there it is electrostatic interactions associated between the metal surface and the charge of the inhibitor molecule i.e. physisorption and if the value of  $\Delta G_{\text{ads}}$ , is equal to -40 kJ/mol or more in negative value, this will be related to the charge transfer from inhibitor molecule to the mild steel surface to form a coordinate type of interaction i.e. chemisorption [24-25]. In the present study the values of  $\Delta G_{\text{ads}}$  are around -42 kJ/mol which suggest the chemisorption mode of adsorption of KA2 and KA3 inhibitors.

### 3.1.3 Potentiodynamic polarization study

Electrochemical tests methods can be used to characterize corrosion mechanisms and predict corrosion rates. The effect of KA2 and KA3 concentration on the potentiodynamic anodic and cathodic polarization curves of mild steel has been studied in 1.0 M HCl solutions. For electrochemical measurements, the inhibition efficiency is calculated using the corrosion current density as follows [26]:

$$\eta = 100 \times \left(1 - \frac{i_{\text{corr}}}{i_{\text{corr}}^{\circ}}\right) \quad (6)$$

$i_{\text{corr}}^{\circ}$  and  $i_{\text{corr}}$  are the corrosion current density values without and with various concentrations of the studied inhibitors, respectively. These values were determined by extrapolation of the cathodic Tafel lines to the corrosion potential. Electrochemical parameters such as, corrosion current densities ( $I_{\text{corr}}$ ), corrosion potentials ( $E_{\text{corr}}$ ), Tafel slope constants that has been calculated from Tafel plots ( $\beta_c$ ) and the inhibition efficiency ( $E\%$ ) are given in Table 3 and shown in figures 4 and 5.

It is clearly noticed in Figures and 5, that in the presence of the inhibitor the curves are shifted towards lower current regions, showing the inhibition tendency of inhibitors. The cathodic current potential curves gave rise to parallel Tafel lines, which indicate that the hydrogen evolution reaction is activation controlled and that the addition of the inhibitor does not modify the mechanism of this process. Figures 4 and 5, also reveal that the presence of the inhibitor affects the anodic dissolution of mild steel as well as the cathodic reduction of hydrogen ions. The decrease in the current density ( $I_{\text{corr}}$ ) increases the inhibition efficiency of the inhibitor. Both the cathodic Tafel slopes, namely  $\beta_a$  are varying from the blank values indicating the cathodic mode of inhibition.

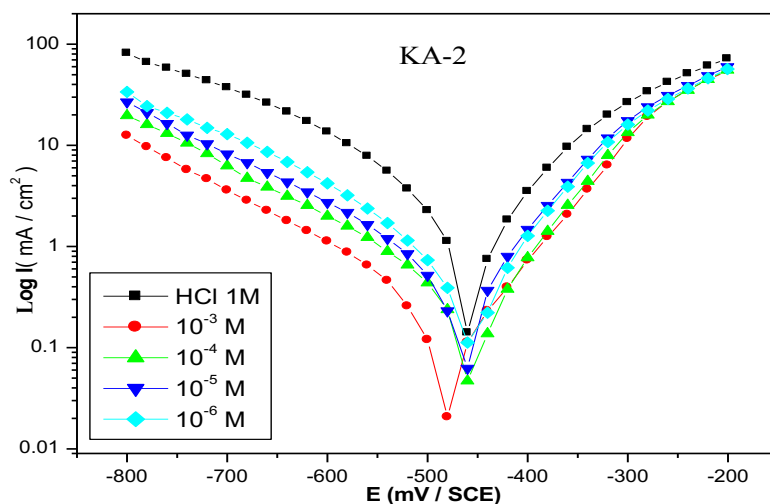


Figure 4: Polarization curves of mild steel in 1.0 M HCl solution with different concentrations of KA2.

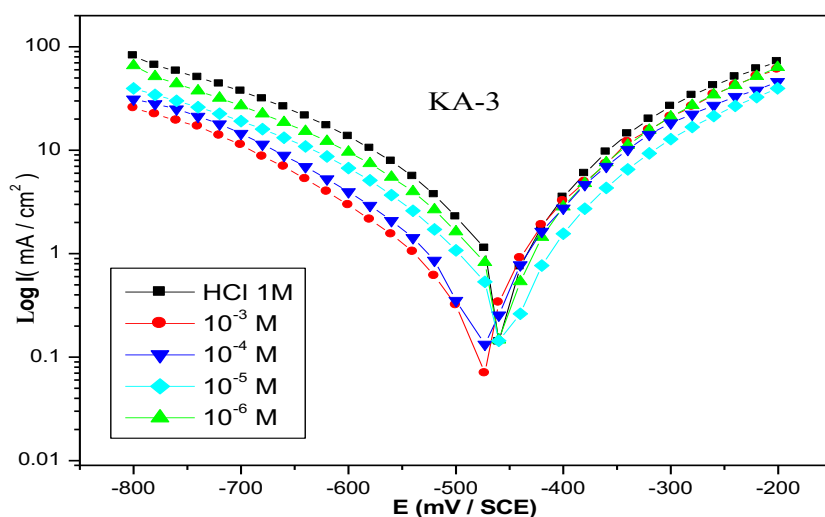


Figure 5: Polarization curves of mild steel in 1.0 M HCl solutions with different concentrations of KA3.

Table 3: Electrochemical parameters of mild steel in 1.0 M HCl solutions in the presence of different concentrations of the inhibitors KA2 and KA3 at 308 K.

Inhibitor	C (M)	$-E_{\text{corr}}$ (mV/SCE)	$I_{\text{corr}}$ ( $\mu\text{A}/\text{cm}^2$ )	$-\beta_c$ ( $\mu\text{A}/\text{cm}^2$ )	$\eta$ (%)
1.0 M HCl	-	453	1386	173	--
KA2	$10^{-6}$	459	554	192	60
	$10^{-5}$	462	421	183	70
	$10^{-4}$	460	356	164	74
	$10^{-3}$	493	219	171	<b>84</b>
KA3	$10^{-6}$	454	498	177	64
	$10^{-5}$	455	307	179	78
	$10^{-4}$	466	232	182	83
	$10^{-3}$	465	111	169	<b>92</b>

The inhibition efficiency  $\eta$  % increases with the increase in inhibitor concentration to attain a maximum value of 84%, and 92% at  $10^{-3}$  M for KA2 and KA3, respectively. This indicates that these inhibitors act as good inhibitors for mild steel in 1.0 M HCl solutions. Therefore, it could be concluded that KA2 and KA3 adsorb on

both anodic and cathodic sites of the mild steel surface. The electrochemical processes on the mild steel surface are likely to be closely related to the adsorption of the inhibitors, and the adsorption depends on the chemical structure of the inhibitor.

### 3.1.4 Electrochemical impedance spectroscopy

The effect of the concentration of the studied inhibitors KA2 and KA3 was studied from  $10^{-3}$  M to  $10^{-6}$  M in 1.0 M HCl solutions at 308K. Organic compounds are known to yield unreliable and irreproducible results for concentrations higher than  $10^{-3}$  M [27]. For the same reasons, the present work will test the compounds only up to a concentration of  $10^{-3}$  M.

In the presence of the studied inhibitors and in the whole concentration range, the electrochemical impedance spectra (Nyquist plots) are characterized by one semicircle, whose center lies under the real axis (Figures 6 and 7). The parameters deduced are grouped in Table 4. Charge-transfer resistance values ( $R_t$ ) and double layer capacitance values ( $C_{dl}$ ) have been obtained from impedance measurements as described previously. The following relation is used to calculate  $\eta$  (%):

$$\eta\% = 100 \times \left( 1 - \frac{R_{ct}^{\circ}}{R_{ct}} \right) \quad (7)$$

Where  $R_{ct}^{\circ}$  and  $R_{ct}$  are the charge-transfer resistance values with and without various concentrations of the inhibitor, respectively. The values of the double-layer capacitance associated with the loop and the frequency at which the imaginary component of the impedance is maximal ( $-Z_{max}$ ) are calculated from the following relation:

$$C_{dl} = 1/2 \cdot \pi \cdot f_{max} \cdot R_{ct} \quad (8)$$

where  $R_{ct}$  is the diameter of the loop and  $f_{max}$  is the value of the frequency.

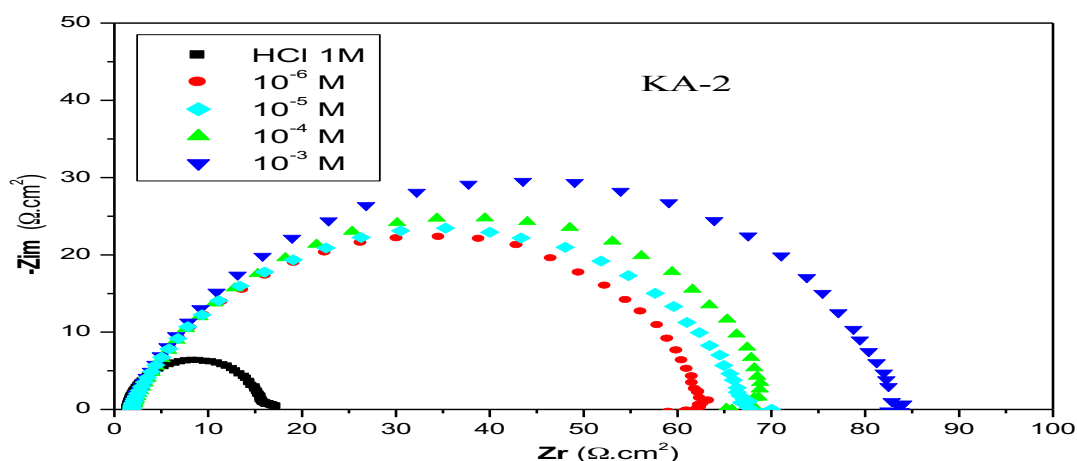


Figure 6: Nyquist diagrams for mild steel in 1.0 M HCl solutions containing different concentrations of KA2.

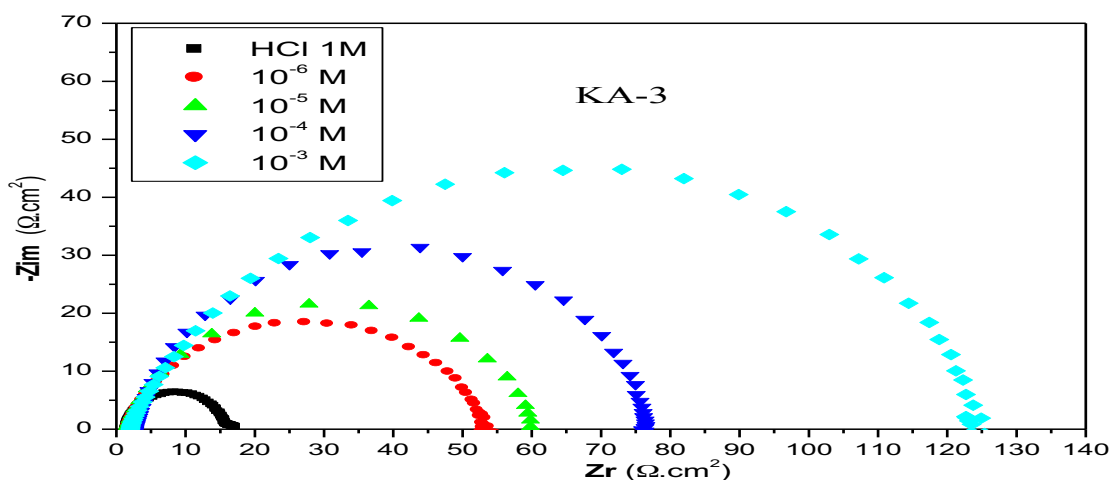


Figure 7: Nyquist diagrams for mild steel in 1.0 M HCl solutions containing different concentrations of KA3.

Examination of Table 4 reveals that, as the concentration of the inhibitor increases, the  $R_{ct}$  rises to higher value showing that KA2 and KA3 inhibit corrosion reaction. The decrease of  $C_{dl}$  is interpreted by the adsorption of KA2 and KA3 molecules on the metal surface. The results obtained from the polarization technique in 1.0 M HCl solution were in good agreement with those obtained from the electrochemical impedance spectroscopy (EIS) with a small variation. The Nyquist diagrams (Figures 6 and 7) show that in the absence and presence of inhibitors at all concentrations, a single semicircle with only one capacitive loop in the entire frequency range.

**Table 4:** Impedance parameters for mild steel in 1.0 M HCl solutions in the absence and presence of different concentrations of KA2 and KA3 at 308 K.

Inhibitors	C (mol/l)	$R_{ct}$ ( $\Omega \cdot \text{cm}^2$ )	$C_{dl}$ ( $\mu\text{f}/\text{cm}^2$ )	$\eta$ (%)
1.0 M HCl	--	15	200	--
KA2	$10^{-6}$	60	137	75
	$10^{-5}$	65	99	77
	$10^{-4}$	79	75	81
	$10^{-3}$	84	71	82
KA3	$10^{-6}$	52	149	71
	$10^{-5}$	61	102	75
	$10^{-4}$	77	73	81
	$10^{-3}$	124	66	88

As shown in Table 4, the value of  $R_{ct}$  increases and  $C_{dl}$  decreases with increasing the inhibitors concentration, which is attributed to the increase in the thickness of the electric double layer on the metal/solution interface and/or decrease in the value of dielectric constant due to the displacement of pre-adsorbed water molecules by the inhibitor molecules. From Table 4, the inhibition performance order of the studied inhibitors is KA3 > KA2.

It is evident that it cannot describe the observed depression of the capacitive loop and it is necessary to replace the capacitor by some element taking into account frequency dispersion like the Constant Phase Element (CPE). This element is a generalized tool, which can reflect exponential distribution of the parameters of the electrochemical reaction related to energetic barrier at charge and mass transfer. Such phenomena often correspond to surface heterogeneity which may be the result of surface roughness, dislocations, distribution of the active sites or adsorption of inhibitors. In order to fit and analyze the EIS data, the equivalent circuit shown in Fig. 9 is selected [28].

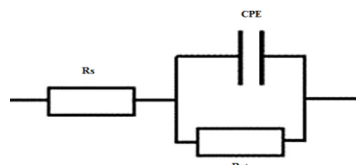


**Figure 9:** Suggested equivalent circuit model of the interface mild steel/1.0 M HCl without and with various concentrations of the studied inhibitors.

### 3.2 Quantum chemical calculations

Quantum chemical calculations are used to correlate experimental data for inhibitors obtained from different techniques (viz., electrochemical and weight loss) and their structural and electronic properties. According to Koopman's theorem [29],  $E_{HOMO}$  and  $E_{LUMO}$  of the inhibitor molecule are related to the ionization potential (I) and the electron affinity (A), respectively. The ionization potential and the electron affinity are defined as  $I = -E_{HOMO}$  and  $A = -E_{LUMO}$ , respectively. Then absolute electronegativity ( $\chi$ ) and global hardness ( $\eta$ ) of the inhibitor molecule are approximated as follows [30]:

$$\chi = \frac{I+A}{2}, \quad \chi = -\frac{1}{2}(E_{HOMO} + E_{LUMO}) \quad (9)$$

$$\eta = \frac{I-A}{2}, \quad \eta = -\frac{1}{2}(E_{HOMO} - E_{LUMO}) \quad (10)$$

Where  $I = -E_{HOMO}$  and  $A = -E_{LUMO}$  are the ionization potential and electron affinity respectively.

The fraction of transferred electrons  $\Delta N$  was calculated according to Pearson theory [31]. This parameter evaluates the electronic flow in a reaction of two systems with different electronegativities, in particular case; a metallic surface (Fe) and an inhibitor molecule.  $\Delta N$  is given as follows:

$$\Delta N = \frac{\chi_{Fe} - \chi_{inh}}{2(\eta_{Fe} + \eta_{inh})} \quad (11)$$

Where  $\chi_{\text{Fe}}$  and  $\chi_{\text{inh}}$  denote the absolute electronegativity of an iron atom (Fe) and the inhibitor molecule, respectively;  $\eta_{\text{Fe}}$  and  $\eta_{\text{inh}}$  denote the absolute hardness of Fe atom and the inhibitor molecule, respectively. In order to apply the eq. 11 in the present study, a theoretical value for the electronegativity of bulk iron was used  $\chi_{\text{Fe}} = 7$  eV and a global hardness of  $\eta_{\text{Fe}} = 0$ , by assuming that for a metallic bulk  $I = A$  because they are softer than the neutral metallic atoms [31].

The electrophilicity has been introduced by Sastri et al. [32], is a descriptor of reactivity that allows a quantitative classification of the global electrophilic nature of a compound within a relative scale. They have proposed the  $\omega$  as a measure of energy lowering owing to maximal electron flow between donor and acceptor and  $\omega$  is defined as follows:

$$\omega = \frac{\chi^2}{2\eta} \quad (12)$$

The softness  $\sigma$  is defined as the inverse of the  $\eta$  as follows [33]:

$$\sigma = \frac{1}{\eta} \quad (13)$$

Using left and right derivatives with respect to the number of electrons, electrophilic and nucleophilic Fukui functions for a site  $k$  in a molecule can be defined in the following equations [34].

$$f_k^+ = P_k(N+1) - P_k(N) \quad \text{for nucleophilic attack} \quad (14)$$

$$f_k^- = P_k(N) - P_k(N-1) \quad \text{for electrophilic attack} \quad (15)$$

$$f_k^{\cdot} = [P_k(N+1) - P_k(N-1)] \frac{1}{2} \quad \text{for radical attack} \quad (16)$$

where,  $P_k(N)$ ,  $P_k(N+1)$  and  $P_k(N-1)$  are the natural populations for the atom  $k$  in the neutral, anionic and cationic species, respectively.

### 3.3 Computational theoretical studies

The FMOs (HOMO and LUMO) are very important for describing chemical reactivity. The HOMO that have no electrons, represents the ability of ( $E_{\text{HOMO}}$ ) to donate an electron, whereas, the LUMO haven't not electrons, represents the ability of ( $E_{\text{LUMO}}$ ) to accept or gain an electron. The energy gap between HOMO and LUMO determines the kinetic stability, chemical reactivity, optical polarizability and chemical hardness–softness of a compound [35].

In this study, the HOMO and LUMO orbital energies were calculated using B3LYP method with 6-31G which is implemented in Gaussian 09 packadge [36-37]. All other calculations were performed using the results with some assumptions. The higher values of  $E_{\text{HOMO}}$  indicate an increase for the electron donor and this means a better inhibitory activity with increasing adsorption of the inhibitor on a metal surface, whereas  $E_{\text{LUMO}}$  indicates the ability of the molecule to accept electron. The adsorption ability of the inhibitor to the metal surface increases with increasing of  $E_{\text{HOMO}}$  and decreasing of  $E_{\text{LUMO}}$ . The HOMO and LUMO orbital energies of KA2 and KA3 inhibitors were performed and were tabulated in Table 6 and shown in Figure 11. High ionization energy ( $> 6$  eV) indicates high stability of KA2 and KA3 inhibitors [38], the number of electrons transferred ( $\Delta N$ ), dipole moment, ionisation potential, electron affinity, electronegativity, hardness, softness and total energy were also calculated and tabulated in Table 6.

**Table 6:** Quantum chemical parameters for KA2 and KA3 obtained in gaseous and aqueous phases with the DFT at the B3LYP/6-31G level.

Parameters	Gaseous Phase		Aqueous Phase	
	KA2	KA3	KA2	KA3
Total Energy $TE$ (eV)	-84978.2	-84933.6	-84978.5	-84934.1
$E_{\text{HOMO}}$ (eV)	-6.9696	-7.5630	-7.0964	-7.4550
$E_{\text{LUMO}}$ (eV)	-0.1107	-0.7622	-0.0035	-0.9978
Gap $\Delta E$ (eV)	6.8588	6.8009	7.0928	6.4572
Dipole moment $\mu$ (Debye)	6.2504	6.6155	8.3457	8.7352
Ionisation potential $I$ (eV)	6.9696	7.5630	7.0964	7.4550
Electron affinity ( $A$ )	0.1107	0.7622	0.0035	0.9978
Electronegativity ( $\chi$ )	3.5402	4.1626	3.5500	4.2264
Hardness ( $\eta$ )	3.4294	3.4004	3.5464	3.2264
Electrophilicity index ( $\omega$ )	1.8272	2.5478	1.7767	2.7663
Softness ( $\sigma$ )	0.2916	0.2941	0.2820	0.3097
Fractions of electron ( $\Delta N$ )	0.5044	0.4172	0.4864	0.4295

The electrophilicity index ( $\omega$ ) is higher for the KA3 product than for KA2, an indication of the electron deficient nature of the KA2 inhibitor. The energy gap  $\Delta E$  is larger for the KA2 than for their KA3 counterparts providing therefore a low reactivity to the KA3. The  $E_{\text{HOMO}}$  in aqueous phase is higher in the KA3 than in the KA2, an indication that acetylene group (C-C triple bond) increases the electron donating capacity of the KA3 inhibitor compared with ethylene group (-C=C-) in KA2.

The value of  $\Delta N$  (number of electrons transferred) show that the inhibition efficiency resulting from electron donation agrees with Lukovit's study [39]. If  $\Delta N < 3.6$ , the inhibition efficiency increases by increasing electron donation ability of these inhibitors to donate electrons to the metal surface [40]. The values of  $\Delta N$  of KA3 (0.4172 and 0.4295 in the gaseous and aqueous phases, respectively) are lower than the values of KA2 (0.5044 and 0.4864 in the gaseous and aqueous phases, respectively), this indicates that KA3 is a better electron donor compared with KA2.

Tables 7 and 8 display the most relevant values of the natural population ( $P(N)$ ,  $P(N-1)$  and  $P(N+1)$ ) with the corresponding values of the Fukui functions ( $f_{k+}$ ,  $f_{k-}$  and  $f_{k^0}$ ) of the studied inhibitors. The calculated values of the  $f_{k+}$  for both inhibitors are mostly localized on the imidazo[4,5-b]pyridine ring, namely C3, C4, C6, Br9 and N22 (KA2) and C3, C6, Br9 and N17 (KA3), indicating that the imidazo[4,5-b]pyridine ring will probably be the favorite site for nucleophilic attacks.

**Table7.** Pertinent natural populations and Fukui functions of KA2 calculated at B3LYP/6-31G in the gaseous (G) and aqueous phases.

	Phase	$P(K)$	$P(K-1)$	$P(K+1)$	$f$	$f^+$	$f^0$
C <sub>3</sub>	G	6.25723	6.39117	6.25576	0.1339	0.0015	0.0677
	A	6.24538	6.43996	6.23418	0.1946	0.0112	0.1029
C <sub>4</sub>	G	6.16306	6.26852	6.08737	0.1055	0.0757	0.0906
	A	6.16531	6.19216	6.09926	0.0269	0.0660	0.0465
C <sub>6</sub>	G	5.55418	5.68799	5.43815	0.1338	0.1160	0.1249
	A	5.5378	5.65552	5.42617	0.1177	0.1116	0.1147
Br <sub>9</sub>	G	34.93895	35.0162	34.69995	0.0772	0.2390	0.1581
	A	34.94556	35.06276	34.70756	0.1172	0.2380	0.1776
N <sub>22</sub>	G	7.43388	7.53839	7.38241	0.1045	0.0515	0.0780
	A	7.45989	7.61834	7.42763	0.1585	0.0323	0.0954

**Table8:** Pertinent natural populations and Fukui functions of KA3 calculated at B3LYP/6-31G in the gaseous (G) and aqueous phases.

	Phase	$P(K)$	$P(K-1)$	$P(K+1)$	$f$	$f^+$	$f^0$
C <sub>3</sub>	G	6.25528	6.41103	6.2079	0.1558	0.0474	0.1016
	A	6.23804	6.4194	6.18402	0.1814	0.0540	0.1177
C <sub>6</sub>	G	5.56661	5.6997	5.47179	0.1331	0.0948	0.1140
	A	5.54585	5.67244	5.46208	0.1266	0.0838	0.1052
Br <sub>9</sub>	G	34.9204	35.03451	34.69791	0.1141	0.2225	0.1683
	A	34.92074	35.00286	34.71907	0.0821	0.2017	0.1419
N <sub>17</sub>	G	7.41442	7.56004	7.31918	0.1456	0.0952	0.1204
	A	7.46897	7.63002	7.37123	0.1611	0.0977	0.1294

The geometry of KA2 and KA3 in the gaseous and aqueous phases (Figure 11) were fully optimized using DFT based on Beck's three parameter exchange functional and Lee–Yang–Parr nonlocal correlation functional (B3LYP) [41-43] and the 6-31G. The optimized molecular and selected angles, dihedral angles and bond lengths of P1 and P2 are given in figure 11. The optimized structure shows that the molecule P1 and have a non-planar structure. The HOMO and LUMO electrons density distributions of KA2 and KA3 are given in Table 9.

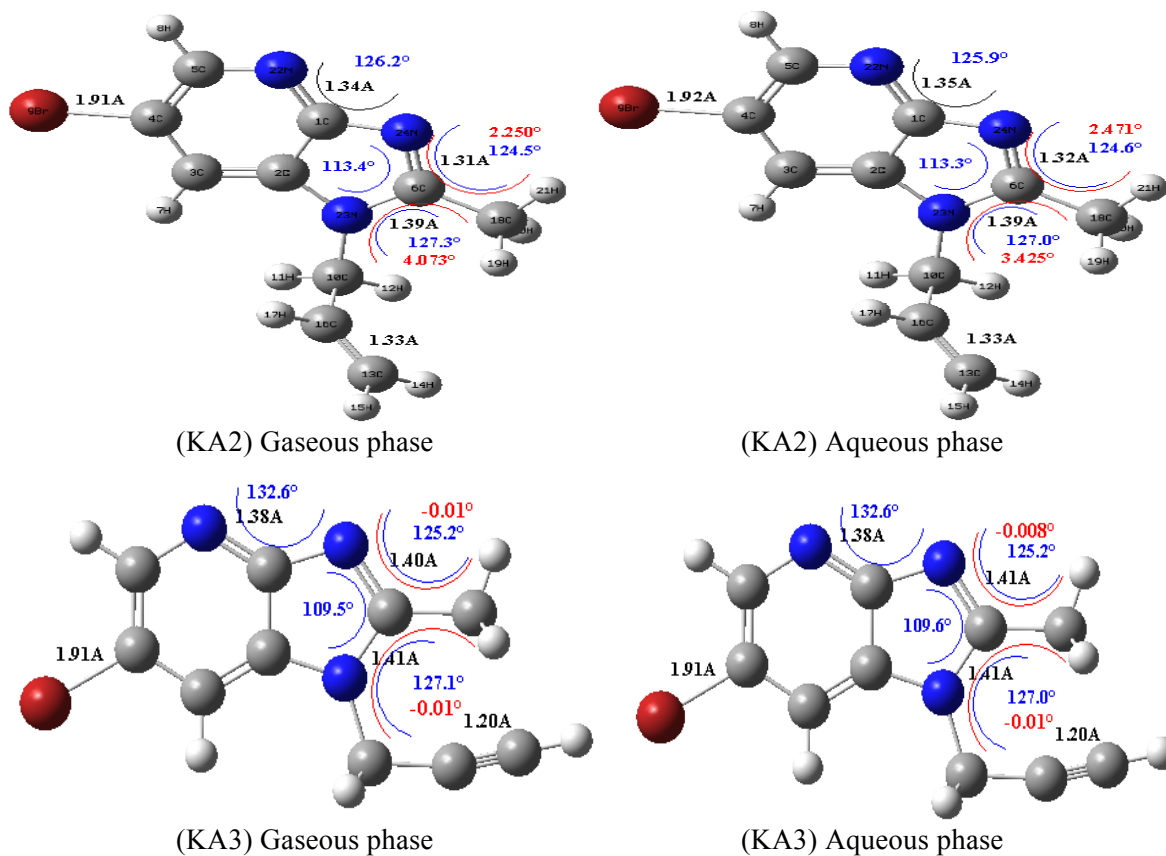
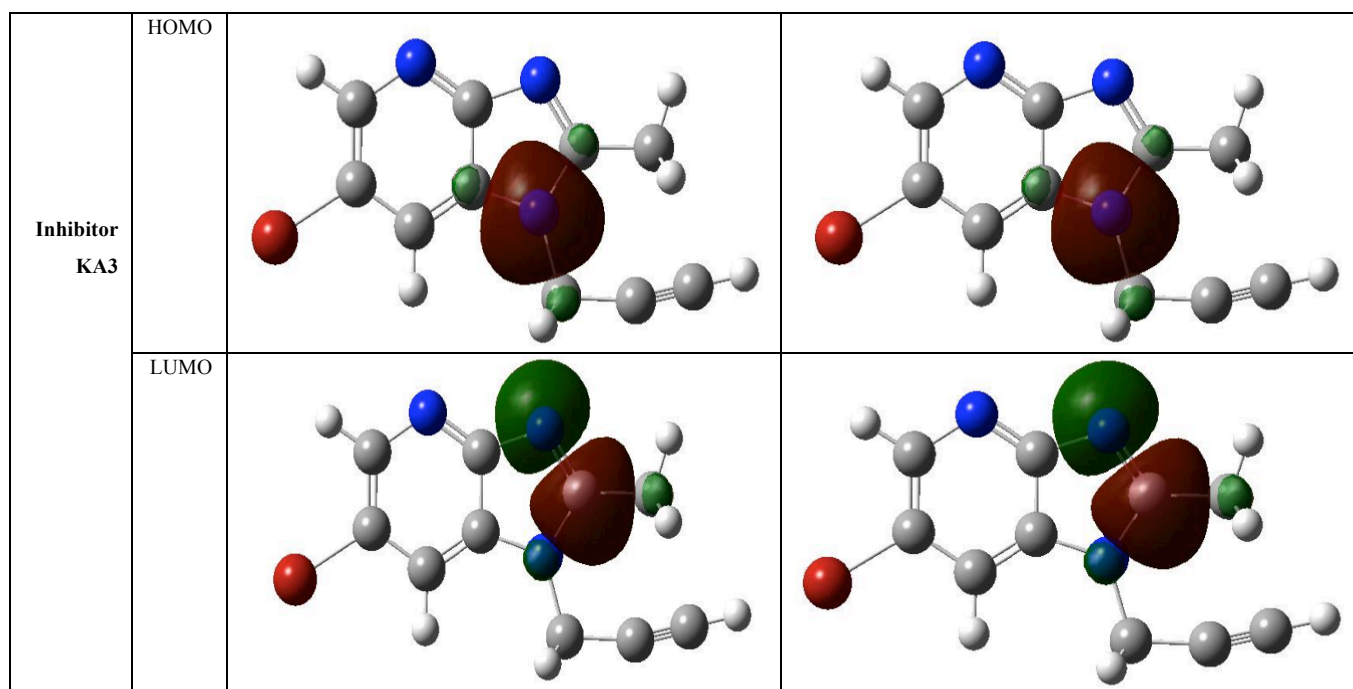


**Figure 11:** Optimized molecular structures and selected dihedral angles (red), angles (blue) and bond lengths (black) of the studied inhibitors calculated in the gaseous and aqueous phases with the DFT at the B3LYP/6-31G level

**Table 9:** The HOMO and the LUMO electrons density distributions of KA2 and KA3 in the gaseous and aqueous phases computed at B3LYP/6-31G level for neutral forms.

		Gaseous Phase	Aqueous Phase
Inhibitor KA2	HOMO		
	LUMO		



## Conclusion

Corrosion inhibition characteristics of the KA2 and KA3 inhibitors have been investigated on mild steel in 1.0 M HCl media and the following conclusions were drawn from the obtained results:

1. The imidazo[4,5-b]pyridine derivatives (KA2 and KA3) acted as a potential corrosion inhibitors for mild steel in 1.0 M HCl solutions and the inhibition efficiency increases with the increase of the concentration of both inhibitors.
2. The absorption of KA2 and KA3 inhibitors on the mild steel surface complies with the Langmuir isotherm mechanism.
3. Potentiodynamic polarization studies have shown that the studied inhibitors KA2 and KA3 act as cathodic-type inhibitors, and their inhibition mechanism is adsorption.
3. Both polarization and EIS studies revealed that both inhibitors are good inhibitors for mild steel corrosion in 1.0 M HCl solution.
4. Quantum chemical calculations provided more detailed accounts of how different electron donating and accepting substituents tuned the extent and mode of the donor-acceptor interactions between the mild steel and the inhibitor molecules and the predicted change in the adsorption free energy values correlate with the experimental inhibition efficiency.

## References

1. P.B. Raja, M.G. Sethuraman, *Mater. Lett.* 62 (2008) 113.
2. H. Elmsellem, H. Nacer, F. Halaimia, A. Aouniti, I. Lakehal, A. Chetouani, B. Hammouti, *Int. J. Electrochem. Sci.* 9 (2014) 5328-5351.
3. M. Lebrini, F. Robert, C. Roos, *Int. J. Electrochem. Sci.* 6 (2011) 847.
4. X. Li, S. Deng, H. Fu, X. Xie, *Corros. Sci.* 78 (2014) 29.
5. M. Lebrini, F. Robert, C. Roos, *Int. J. Electrochem. Sci.* 5 (2010) 1698.
6. M. Faustin, M. Lebrini, F. Robert, C. Roos, *Int. J. Electrochem. Sci.* 6 (2011) 4095.
7. Y. Feng, S. Chen, W. Guo, Y. Zhang, G. Liu, *J. Electroanal. Chem.* 602 (2007) 115-122.
8. R. Salim, E. Ech Chihbi, H. Oudda, Y. ELAoufir, F. El-Hajjaji, A. Elaattiaoui, A. Oussaid, B. Hammouti, H. Elmsellem and M. Taleb, *Der Pharma Chemica*, 8(13) (2016) 200-213
9. L.M. Rodriguez, W. Villamir, L. Martinez, *Corros. Sci.* 48 (2006) 4053.
10. M. Lebrini, F. Bentiss, N. Chihib, C. Jama, J.P. Hornez, M. Lagrenée, *Corros. Sci.* 50 (2008) 2914.
11. A. Zarrouk, B. Hammouti, T. Lakhlifi, M. Traisnel, H. Vezin, F. Bentiss, *Corros. Sci.* 90 (2015) 572-584.
12. D.A. Lopez, S.N. Simison, S.R. deSanchez, *Electrochim. Acta* 48 (2003) 845.
13. A. Elyoussfi, A. Dafali, H. Elmsellem, H. Steli, Y. Bouzian, K. Cherrak, Y. El Ouali, A. Zarrouk, B. Hammouti, *J. Mater. Environ. Sci.* 7 (2016) 3344.

14. M. Lebrini, F. Bentiss, N. Chihib, C. Jama, J.P. Hornez, M. Lagrenée, *Corros. Sci.* 50 (2008) 2914.
15. M. Ramdani, H. Elmsellem, N. Elkhiaati, B. Haloui, A. Aouniti, M. Ramdani, Z. Ghazi, A. Chetouani, and B. Hammouti, *Der Pharma Chemica*, 7 (2015) 67-76.
16. F. Aouinti, H. Elmsellem, A. Bachiri, M-L. Facounnier, A. Chetouani, C. Belbachir, A. Aouniti, and B. Hammouti, *Journal of Chemical and Pharmaceutical Research*, 6 (2014) 10-23.
17. P. Udhayakala, T.V. Rajendiran, S. Gunasekaran, *Journal of Chemical, Biological and Physical Sciences A*, 2 (2012) 1151-1165.
18. R.K. Roy, S. Pal, K. Hirao, *J. Chem. Phys.*, 110(1999)8236.
19. W. Li, Q.He, C. Pei, B.Hou, *Electrochim. Acta.* 52 (2007) 6386-6394.
20. H. Elmsellem, N. Basbas, A. Chetouani, A. Aouniti, S. Radi, M. Messali, B. Hammouti, *Portugaliae Electrochimica Acta*, 32 (2014) 77-108.
21. A. Elyoussfi, H. Elmsellem, A. Dafali, K. Cherrak, A. Zarrouk, B. Hammouti, *Der Pharma Chemica*. 7 (2015) 284-291.
22. H. Elmsellem, T. Harit, A. Aouniti, F. Malek, A. Riahi, A. Chetouani, B. Hammouti, *Protection of Metals and Physical Chemistry of Surfaces*. 51 (2015) 873.
23. H. Bendaha, H. Elmsellem, A. Aouniti, A. Chetouani, B. Hammouti, *Physicochemical Mechanics of Materials*, 1 (2016) 111-118.
24. R. Chadli, A. ELherri, H. Elmsellem, M. Elazzouzi, N. Merad, A. Aouniti, B. Hammouti, J. K. Mulengi and A. Zarrouk. *Protection of Metals and Physical Chemistry of Surfaces*. 53 (2017) 928–936.
25. M. Lebrini, F. Robert, A. Lecante, C. Roos, *Corros. Sci.* 53 (2011) 687.
26. L. Essaghoulani, M. Ellouz, M. El Hafi, M. Boulhaoua, N. K. Sebbar, E. M. Essassi, M. Bouabdellaoui, A. Aouniti and B. Hammouti, *Der Pharma Chemica*. 8 (2016) 297-305.
27. A.K. Singh, M.A. Quraishi, *Corros. Sci.* 53 (2011) 1288.
28. F. Xu, J. Duan, S. Zhang, & B. Hou, *Materials Letters*, 62 (2008) 4072-4074.
29. R.G. Pearson, *Inorg. Chem.* 27 (1988) 734-740.
30. R. G. Parr, W. Yang, *Density-Functional Theory of Atoms and Molecules*. Oxford University Press, New York, (1989).
31. T. A. Carlson, C.W. Nestor Jr., N.Wasserman and J.D. Mcdowell, *Atomic Data and Nuclear Data Tables*, 2 (1970) 63–99.
32. V.S Sastri, J.R Perumareddi, *Corrosion*, 53 (1997) 617–622.
33. P. Udhayakala, T. V. Rajendiran, S. Gunasekaran, *Journal of Chemical, Biological and Physical Sciences A*, 2(2012)1151–1165.
34. R.K. Roy, S. Pal, K. Hirao, *J. Chem. Phys.* 110 (1999) 8236.
35. M. Govindarajan, M. Karabacak, *SpectrochimActa Part A Mol. Biomol. Spectrosc.*, 85 (2012) 251-60.
36. A. D. Becke, *J. Chem. Phys.* 98 (1993) 1372.
37. L. Essaghoulani, H. Elmsellem, M. Ellouz, M. El Hafi, M. Boulhaoua, N. K. Sebbar, E. M. Essassi, M. Bouabdellaoui, A. Aouniti and B. Hammouti, *Der Pharma Chemica*. 8 (2016) 297-305.
38. D. Jeroundi, S. Chakroune, B. Hammouti, R. Idouhli, E. M. El Hadrami, A. Ben-Tama, M. Oudani, Y. Ouzidan and Y. Kandri Rodi, *J. Mater. Environ. Sci.* 7 (10) (2016) 3895-3905.
39. I. Lukovits, E. Kalman, F. Zucchi, *Corrosion*, 57 (2001) 3-7.
40. R. Chadli, M. Elazouzi, I. Khelladi, A.M. Elhourri, A. Aouniti, J. Kajima Mulengi, B. Hammouti, *Portugaliae Electrochimica Acta*. 35 (2017) 65-80
41. D. Jeroundi, S. Chakroune, R. Idouhli, A. Elyoussfi, A. Dafali, E. M. El Hadrami, A. Ben-Tama, Y. Kandri Rodi, *J. Mater. Environ. Sci.* 7 (11) (2016) 4024-4035.
42. C. Lee, W. Yang, R. G. Parr, *Phys. Rev. B*, 37 (1988) 785.
43. I. Chakib, H. Elmsellem, S. Lahmidi, A. Nadeem, I. Abdel-Rahman, F. Bentiss, B. Hammouti, *J. Mater. Environ. Sci.*, 7 (6) (2016) 1866-1881.

(2018) ; <http://www.jmaterenvirosci.com>